Trojan horse method applied to ^{9}Be$(p,\alpha)^{6}$Li at astrophysical energies

Qun-Gang Wen, Cheng-Bo Li, Shu-Hua Zhou, Qiu-Ying Meng, Jing Zhou, Xiao-Mei Li, Shou-Yang Hu, and Yuan-Yong Fu
China Institute of Atomic Energy, P. O. Box 275(18), Beijing 102413, People's Republic of China

C. Spitaleri, A. Tumino, R. G. Pizzone, and G. G. Rapisarda
Laboratori Nazionali del Sud-INFN, Catania, Italy

(Received 9 April 2008; revised manuscript received 20 June 2008; published 26 September 2008)

The low-energy bare-nucleus cross section for ^{9}Be$(p,\alpha)^{6}$Li has been extracted by means of the Trojan horse method (THM) applied to the ^{2}H(^{9}Be, α,^{6}Li)n reaction at a beam energy of ^{9}Be of 22.35 MeV. For the first time, we assume an intermediate process, $^{9}\mathrm{Be} + {}^{2}\mathrm{H} \rightarrow {}^{9}\mathrm{Be} + p + n$, and considered this process as one criterion of the quasifree condition. Accordingly, sequential decay processes were eliminated. The derived astrophysical $S(E)$ factor for the two-body process ^{9}Be$(p,\alpha)^{6}$Li is compared with that obtained from direct experiments. We have found good agreement between the two results, leading to an improved determination of the $S(E)$ with $S(0) = 21.0 \pm 0.8$ MeV b. Furthermore, the electron screening potential energy $U_e = 676 \pm 86$ eV has also been extracted in a model-independent way by comparing the direct and THM data. The value is significantly higher than that predicted by current theoretical models, whereas it is lower than $Ue \simeq 830$ eV, which was extracted from direct measurements with inclusion of the $E_{\mathrm{c.m.}} = -23$ keV subthreshold resonance.

DOI: 10.1103/PhysRevC.78.035805 PACS number(s): 24.50.+g, 24.10.−i, 25.70.Hi, 26.20.−f

I. INTRODUCTION

The abundances of light elements such as lithium, beryllium, and boron have been increasingly used as diagnostics between different scenarios for primordial or stellar nucleosynthesis [1]. In both stellar and primordial environments, however, Li, Be, and B are mainly destroyed by proton-capture reactions via the (p,α) channel with a Gamow energy E_G ranging from 10 keV (for stellar nucleosynthesis) to 100 keV (for primordial nucleosynthesis). These energies are lower than the Coulomb barrier E_C which is usually on the order of MeV, thus implying that the reactions take place via the tunnel effect with the cross section at nano- or pico- barn. The behavior of the direct cross sections is usually extrapolated from higher energies to the astrophysical energy region by using the definition of the astrophysical factor

$$S(E) = E[\sigma(E)]\exp(2\pi\eta) \tag{1}$$

(where η is the Sommerfeld parameter), which varies smoothly with energies. Nevertheless, this extrapolation procedure can introduce some uncertainties due to, for example, the presence of unexpected subthreshold resonances or electron screening effects [2].

Using the Trojan horse method (THM) [3,4], the quasifree (QF) contribution of a suitable three-body reaction is selected under appropriate kinematic conditions. The energy in the entrance channel of the three-body reaction is chosen well above the Coulomb barrier to extract the two-body cross section at astrophysical energies free of Coulomb suppression.

The ^{9}Be$(p,\alpha)^{6}$Li reaction via the THM has been studied in Ref. [5], which has shown the presence of the expected low-energy resonance at $E_{\mathrm{c.m.}} \sim 0.27$ MeV (corresponding to the 6.87 MeV, $J^{\pi} = 1^{-}$ level of ^{10}B), but no information has been extracted about either the $S(E)$ factor or screening effects. The present work aimed at extracting the $S(E)$ factor and screening effects. Here, for the first time, we assumed that an intermediate process $^{9}\mathrm{Be} + {}^{2}\mathrm{H} \rightarrow {}^{9}\mathrm{Be} + p + n$ exists and considered that the process is a criterion of the quasifree condition.

II. TROJAN HORSE METHOD

The basic idea of the THM is to extract a two-body

$$A + x \rightarrow C + c \tag{2}$$

reaction cross section from the QF contribution of a suitable three-body

$$A + a \rightarrow C + c + b \tag{3}$$

reaction. The nucleus a is considered to be dominantly composed of clusters x and b. After the breakup of a due to the interaction with A, the two-body reaction occurs between the transferred particle x and the nucleus A, whereas the nucleus b acts as a spectator. The energy in the entrance channel $A + a$ can be chosen above the height of the Coulomb barrier, so as to avoid a reduction in the cross section. At the same time, the effective energy of the reaction between A and x can be relatively small, mainly because of the binding energy ε_a of a with respect to the $x + b$ threshold [Eqs. (4) and (5)], and the Fermi motion E_{xb} of x inside a can compensate at least partially for the $A + x$ relative motion [Eq. (6)]. See also Eq. (17).

$$E_{Ax}^{\mathrm{QF}} = E_{Aa}\left(1 - \frac{\mu_{Aa}}{\mu_{Bb}}\frac{\mu_{bx}^{2}}{m_x^{2}}\right) - \varepsilon_a, \tag{4}$$

$$\varepsilon_a = (m_x + m_b - m_a)c^{2}, \tag{5}$$

$$E_{Ax} = E_{Ax}^{qf} \pm E_{xb}. \tag{6}$$

Since the transferred particle x is hidden inside the nucleus a and the collision of A and x takes place in the nuclear interaction region, the two-body reaction isfree of Coulomb suppression and, at the same time, not affected by electron screening effects.

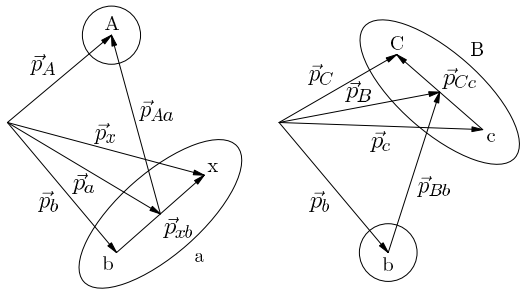

FIG. 1. Coordinate momenta in the initial and final partitions of the Trojan horse reaction, Eq. (3).

The relation of the three-body cross section to the two-body cross section for partialwave l can be written as [4] (see Fig. 1)

$$\frac{d^3\sigma}{dE_{Cc}\,d\Omega_{Bb}\,d\Omega_{Cc}} = \mathrm{KF}|W(\vec{Q}_{Bb})|^2 P_l \frac{d\sigma_l}{d\Omega}(Ax \to Cc), \quad (7)$$

where KF is the kinematical factor

$$\begin{aligned}\mathrm{KF} &= \frac{\mu_{Aa}\mu_{Bb}\mu_{Cc}}{(2\pi)^5\hbar^6}\frac{k_{Bb}k_{Cc}}{k_{Aa}}\frac{16\pi^2}{k_{Ax}^2 Q_{Aa}^2}\frac{v_{Cc}}{v_{Ax}}\frac{k_{Ax}^2}{k_{Cc}^2}\\ &= \frac{\mu_{Aa}\mu_{Bb}\mu_{Ax}}{2\pi^3\hbar^6}\frac{k_{Bb}}{k_{Aa}k_{Ax}Q_{Aa}^2}.\end{aligned} \quad (8)$$

The quantities $\vec{Q}_{Aa}$ and $\vec{Q}_{Bb}$ are given by

$$\vec{Q}_{Aa} = \vec{k}_{Aa} - \frac{m_A}{m_A + m_x}\vec{k}_{Bb}, \quad (9)$$

$$\vec{Q}_{Bb} = \vec{k}_{Bb} - \frac{m_b}{m_b + m_x}\vec{k}_{Aa}, \quad (10)$$

with the relative momenta $\hbar\vec{k}_{Aa}$ and $\hbar\vec{k}_{Bb}$ in the entrance and exit channels, respectively.

The momentum amplitude W is introduced by a Fourier transformation

$$V_{xb}(r_{xb})\phi_a(\vec{r}_{xb}) = \int \frac{d^3q}{(2\pi)^3} W(\vec{q})\exp(i\vec{q}\cdot\vec{r}_{xb})\phi_x\phi_b \quad (11)$$

of the product of the ground state wave function ϕ_a and the interaction potential V_{xb}. With the help of the Schrödinger equation, the momentum amplitude W is related to the ground state momentum wave function of the nucleus a

$$\Phi_a(\vec{Q}_{Bb}) = \langle \exp(i\vec{Q}_{Bb}\cdot\vec{r}_{xb})\phi_x\phi_b|\phi_a(\vec{r}_{xb})\rangle, \quad (12)$$

by

$$W(\vec{Q}_{Bb}) = -\left(\varepsilon_a + \frac{\hbar^2 Q_{Bb}^2}{2\mu_{xb}}\right)\Phi_a(\vec{Q}_{Bb}). \quad (13)$$

The momentum $\hbar\vec{Q}_{Bb}$ is directly related to the momenta of the spectator and the transferred particle after the breakup. Neglecting the binding energy of the nuclei, the argument of W can be well approximated by $\vec{Q}_{Bb} \approx \vec{k}_{xb}$. For a target a at rest, this is just the negative of the spectator recoil k_b or the momentum k_x of the transferred particle x. Of course, in the actual calculation, the full expression for $\vec{Q}_{Bb}$ is used.

In Eq. (7), P_l is the penetration function [4]

$$\begin{aligned}P_l(R,\eta_{Ax},k_{Ax},Q_{Aa}) \to k_{Ax}^2 R^2 z_l^2(Q_{Aa}R)\big[F_l^2(\eta_{Ax};k_{Ax}R)\\ + G_l^2(\eta_{Ax};k_{Ax}R)\big],\end{aligned} \quad (14)$$

the Sommerfeld parameter $\eta_{Ax} = \frac{Z_A Z_x e^2}{\hbar v_{Ax}}$, F_l and G_l are the regular and irregular Coulomb wave functions, and R is a cutoff radius originating from the plane-wave and surface approximations. In the present case, we have used for R the sum of the nuclear radii, assuming for each nucleus, $r = r_0 A^{1/3}$, with $r_0 = 1.4$ fm.

Energy conservation in the two-body reaction (2) can be expressed as

$$E_{Ax} = E_{Cc} - Q_2, \quad (15)$$

with the Q value

$$Q_2 = (m_A + m_x - m_C - m_c)c^2, \quad (16)$$

and similarly (see Fig. 1)

$$\begin{aligned}E_{Aa} &= E_{Cc} + E_{Bb} - Q_3\\ &= E_{Ax} + E_{Bb} + Q_2 - Q_3\\ &= E_{Ax} + E_{Bb} + \varepsilon_a,\end{aligned} \quad (17)$$

with

$$Q_3 = (m_A + m_a - m_C - m_c - m_b)c^2, \quad (18)$$

in the case of the three-body reaction (3). In an experiment, $\vec{p}_{Aa}$ is fixed, and p_{Bb}, p_{Cc}, and p_{Ax} are functions of the single variable E_{Cc}, while Q_{Aa} and Q_{Bb} are functions of two variables E_{Cc} and $\theta_{Bb} = \arccos(\frac{\vec{k}_{Bb}\cdot\vec{k}_{Aa}}{|k_{Bb}|\cdot|k_{Aa}|})$; i.e., Eq. (7) can be written as

$$\frac{d^3\sigma}{dE_{Cc}\,d\Omega_{Bb}\,d\Omega_{Cc}} \propto f(E_{Cc},\theta_{Bb})\frac{d\sigma_l}{d\Omega}(Ax \to Cc). \quad (19)$$

The aim of the present experiment was to extract the cross section of the $^9\mathrm{Be} + p \to {}^6\mathrm{Li} + \alpha$ reaction after selecting the QF contribution of the $^9\mathrm{Be} + d \to {}^6\mathrm{Li} + \alpha + n$ reaction. The deuteron was used as the Trojan horse nucleus, due to its $p + n$ structure [6]; the proton acts as a participant, while the neutron is a spectator to the virtual two-body reaction.

III. EXPERIMENTS

The experiment was performed at Beijing Tandem Accelerator National Laboratory, of the China Institute of Atomic Energy. A beam of ^{9}Be of 22.35 MeV was provided by the HI-13 tandem accelerator. The beam intensity ranged between 10 and 20 nA. A strip of deuterated polyethylene target (CD_2) of about 155 μg/cm^2 in thickness and 1.5 mm in width was oriented with its surface perpendicular to the beam direction. Using the strip target limited the horizontal width of the beam spot in 1.5 mm to decrease the angle error. A silicon ΔE-E telescope, with a position-sensitive detector (PSD) as E, was placed at about 250 mm from the target at an angle of $-30^\circ(\pm 5^\circ)$ for a continuous monitoring of the target thickness during the experiment. The particle detection was performed by using two position-sensitive detectors. The two PSDs were placed at opposite sides with respect to the beam direction at a

distance from the target $d = 250$ mm. The detection angle was $23^\circ(\pm 5^\circ)$ (PSD1 for α detection) and $-15^\circ(\pm 5^\circ)$ (PSD2 for ^{6}Li detection). The arrangement of the experimental setup was chosen by means of Monte Carlo simulation to cover a region of QF pairs. The trigger for the event acquisition was given by the coincidence of two signals from the two PSDs. Energy and position signals for the detected particles were processed by standard electronics and sent to the acquisition system for online monitoring and data storage for offline analysis.

To perform the position calibration, a grid with a number of equally spaced slits was placed in front of each PSD. A correspondence between the position signals from the PSDs and the detection angles of the particles was then established. The energy calibration was performed by means of a standard α source, the ^{12}C(^{6}Li, ^{6}Li)^{12}C and ^{197}Au(^{6}Li, ^{6}Li)^{197}Au reactions with ^{6}Li beam at 16 and 8 MeV, and the ^{197}Au(^{9}Be, ^{9}Be)^{197}Au reaction with ^{9}Be beam at 22.35 MeV.

IV. DATA ANALYSIS

A. Three-body reaction identification

After position and energy calibration, we need to select ^{6}Li and α particles detected in coincidence. A three-body reaction satisfies Eq. (17). In the present experiment, the relative energy of incident particles was fixed at E_0. We assume all those particles detected by PSD1 are α with physical quantity footnotes being 1, all particles detected by PSD2 are ^{6}Li with physical quantity footnotes being 2, and the third particles calculated with ^{2}H(^{9}Be, α, ^{6}Li)n three-body reaction kinematic equations are n with physical quantity footnotes being 3. In a two-dimensional plot of E_{1-23} (relative energy of α and the whole of ^{6}Li and n) vs E_{2-3}(relative energy of ^{6}Li and n), the three-body events will fall in a line with a slope of -45° when the events are consistent with the assumption we made. From Fig. 2 we can find this line from the experimental data. The corresponding Q-value spectrum is shown in Fig. 3, where one can see a peak centered about -0.1 MeV according to the expected theoretical value. Similarly E_{12-3} vs E_{1-2}, or E_{13-2} vs E_{1-3} fall in a line with a slope of -45°.

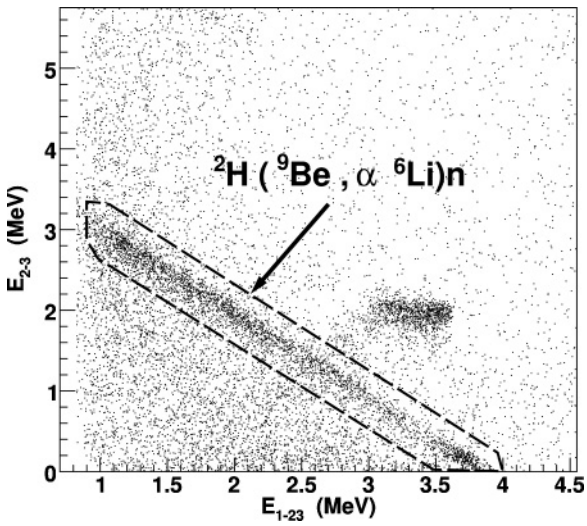

FIG. 2. Kinematic locus of events E_{2-3} vs E_{1-23}.

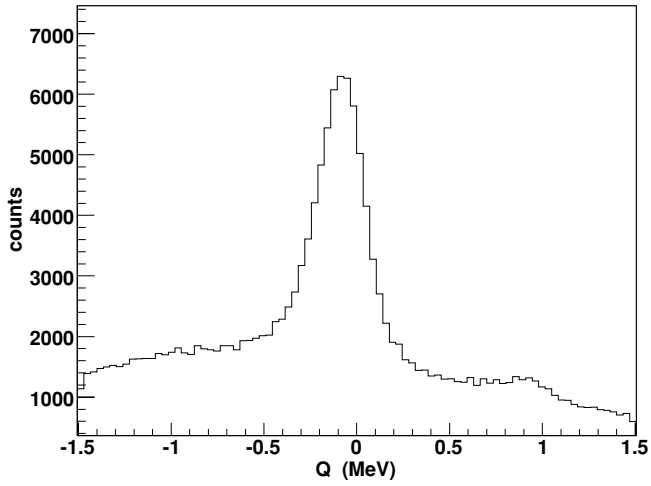

FIG. 3. Q-value spectrum corresponding to the kinematic locus of Fig. 2. The sharp peak, around -0.1 MeV, corresponds to the three-body reaction ^{2}H(^{9}Be, α,^{6} Li)n.

Those events within the graphical cut in Fig. 2 were selected as ^{2}H(^{9}Be, α,^{6} Li)n reaction events. The number of events for PSD1 detecting α and PSD2 detecting ^{6}Li is much larger than that for the other way around. This case was considered when we selected the angular ranges covered by PSD1 and PSD2. By simulation, we can select events with PSD1 detecting ^{6}Li and PSD2 detecting α and eliminate them.

B. QF mechanism identification

1. Intermediate process

As shown in Fig. 4, the $^9\mathrm{Be} + {}^2\mathrm{H} \rightarrow {}^6\mathrm{Li} + \alpha + n$ reaction can proceed through different reaction mechanisms. So we need to select those events that fit with the process shown in Fig. 4(a). To do so, we assume the reaction has an intermediate process of $^9\mathrm{Be} + {}^2\mathrm{H} \rightarrow {}^9\mathrm{Be} + p + n$ (see Fig. 5). So we have the following equations

$$\frac{p_{Aa'}^2}{2\mu_{Aa'}} + \frac{p_{bx}^2}{2\mu_{bx}} = \frac{p_{Aa}^2}{2\mu_{Aa}} + Q', \tag{20}$$

$$Q' = (m_a - m_b - m_x)c^2, \tag{21}$$

$$\vec{p}_{bx} - \frac{m_b}{m_{a'}}\vec{p}_{Aa'} + m_b\vec{v}_c = \vec{p}_b. \tag{22}$$

In Eq. (22), $\vec{p}_b$ is the momentum of $b(n)$ in the laboratory system, and $\vec{v}_c = \frac{\vec{p}_{Aa}}{m_a}$ because $a(^2\mathrm{H})$ is at rest in the present experiment.

Using Eqs. (20)–(22), we may calculate $p_{Aa'}$ or p_{bx} with $b(n)$ momentum determined by the experimental data. We assume that the intermediate process $^9\mathrm{Be} + {}^2\mathrm{H} \rightarrow {}^9\mathrm{Be} + p + n$ will occur if the value of $p_{Aa'}$ or p_{bx} is positive real, and we consider this intermediate process as one criterion of the quasifree condition. As a result, one can clearly see in Fig. 6 that those events belonging to the Fig. 4(b) process are accordingly eliminated. After the quasifree conditions selected, we cannot find obviously excited states in Fig. 7, except a level of $E_{^6\mathrm{Li}\text{-}n} = 0.2$ MeV in Fig. 7(b) belonging to

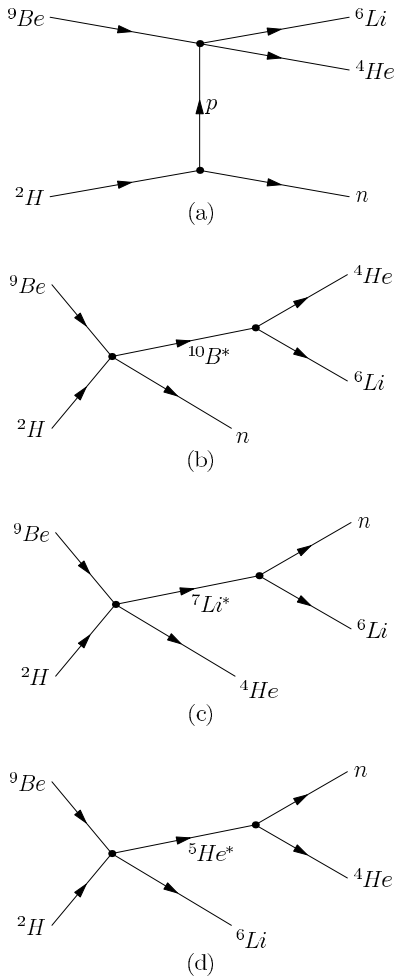

FIG. 4. Different reaction mechanisms leading to the same final state represented by pseudo-Feynman diagrams. A quasifree process is shown in (a), while three different sequential decays are shown in (b), (c), and (d).

the 7.45 MeV excited states of ^{7}Li*. However, it is in the energy range of $E_{^6\text{Li-}\alpha} = 3.1$–$3.6$ MeV, which exceeds the interesting energy range of $E_{^6\text{Li-}\alpha} = 2.125$–$2.425$ MeV [i.e., using Eq. (23), $E_{\text{c.m.}} = 0$–0.3 MeV]. So the level does nothing to the results.

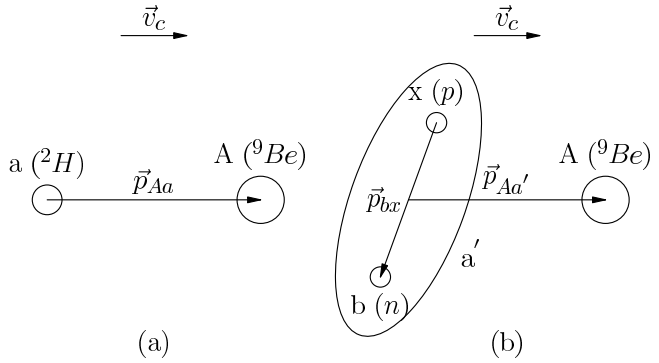

FIG. 5. An intermediate process $^9\text{Be} + ^2\text{H} \rightarrow ^9\text{Be} + p + n$. $\vec{v}_c$ is the velocity in the center-of-mass coordinate.

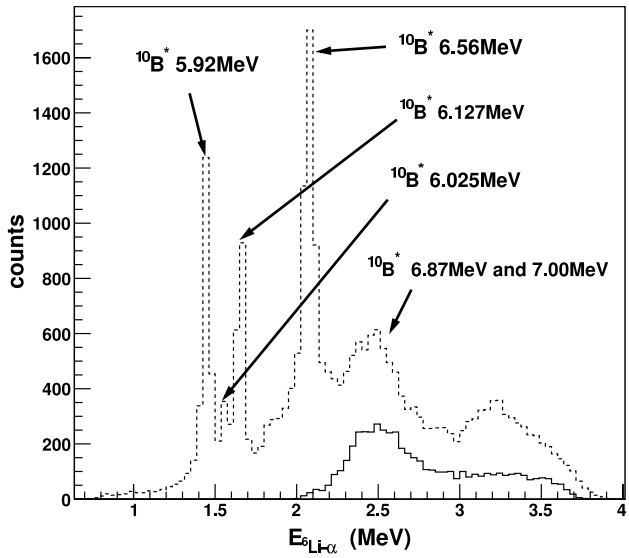

FIG. 6. Solid histogram shows the results restricted by the condition that the assumed intermediate process $^9\text{Be} + ^2\text{H} \rightarrow ^9\text{Be} + p + n$ is one criterion of the quasifree process. Without this restriction, the energy region of the quasifree process overlaps with the energy region of the sequential decay via the 5.92, 6.025, 6.127, 6.56, 6.87, and 7.00 (MeV) compound states in ^{10}B (dashed histogram).

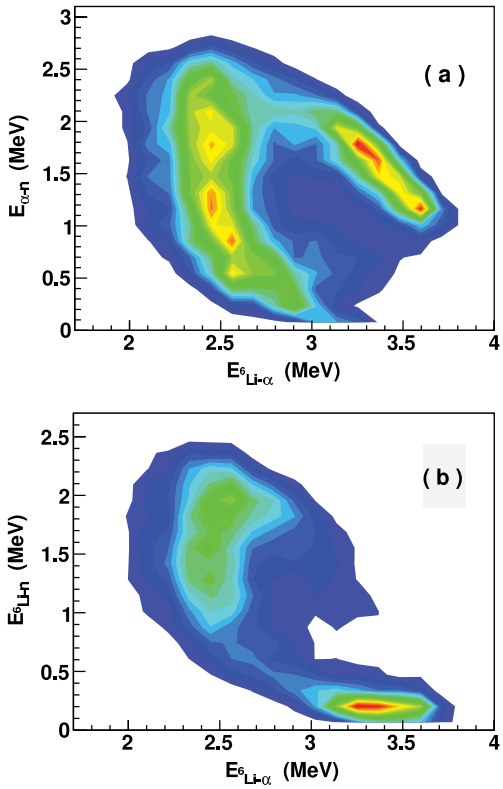

FIG. 7. (Color online) (a) α-n vs ^{6}Li-α and (b) ^{6}Li-n vs ^{6}Li-α relative energy two-dimensional plots after quasifree conditions are selected. If there were levels of ^{5}He*, ^{7}Li*, or ^{10}B*, we should find horizontal lines for ^{5}He* and ^{7}Li* or vertical lines for ^{10}B* in this plot. There is a level of $E_{^6\text{Li-}n} = 0.2$ MeV in (b) belonging to the 7.45 MeV excited states of ^{7}Li*, but it does nothing to the results.

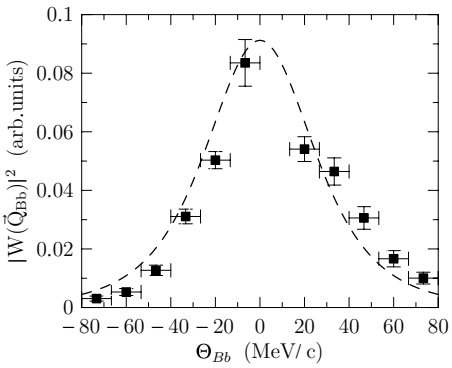

FIG. 8. Comparison between the experimental neutron momentum distribution (square symbols) and theoretical Hulthen function [7] (dashed line). The error bars are due to statistical errors.

2. *Analysis of the neutron momentum distribution*

The term $P_l \frac{d\sigma_l}{d\Omega}$ in Eq. (7) represents the nuclear part of the differential cross section for the virtual two-body reaction ^{9}Be$(p,\alpha)^6$Li that in post-collision prescription occurs at an energy

$$E_{\text{c.m.}} = E_{^6\text{Li-}\alpha} - Q_{2b}, \tag{23}$$

where $E_{^6\text{Li-}\alpha}$ is the ^{6}Li-α relative energy and Q_{2b} is the two-body Q value.

To reconstruct the neutron momentum distribution, a small ^{6}Li-α relative energy window (about 100 keV) was selected. In such a small energy window, $P_l \frac{d\sigma_l}{d\Omega}$ can be considered constant. Thus the experimental $|W(\vec{Q}_{Bb})|^2$ distribution was extracted by dividing the three-body coincidence yield by the kinematic factor. The result is compared with the theoretical one [7] in Fig. 8. The agreement between experimental and theoretical momentum distribution represents a very strong check for the existence of the QF mechanism in the present data.

C. Validity tests for the THM and the astrophysical $S(E)$ factor

After the identification of the QF events, it is necessary to test the validity of the THM. The first test is represented by the comparison between the indirectly extracted angular distributions and the direct behavior. To get the indirect angular distribution, i.e., the emission angle for the α particle in the ^{6}Li-α center-of-mass system, the relevant angle was calculated according to the relation [8]

$$\theta_{\text{c.m.}} = \arccos \frac{(\vec{v}_p - \vec{v}_t)\cdot(\vec{v}_C - \vec{v}_c)}{|\vec{v}_p - \vec{v}_t||\vec{v}_C - \vec{v}_c|}, \tag{24}$$

where the vectors $\vec{v}_p, \vec{v}_t, \vec{v}_C$, and $\vec{v}_c$ are the velocities of projectiles, transferred protons, and outgoing α and ^{6}Li particles, respectively. These quantities can be calculated from their corresponding momenta in the laboratory system, but the transferred protons are of exception. The momentum of the transferred protons is equal and opposite to $\vec{p}_{bx}$ (see Fig. 5) because of the quasifree assumption mentioned above. The angular distributions test was performed for different ^{6}Li-α relative energy intervals and normalized to the direct data [9]. An example of the results is shown in Fig. 9. The error bars include both statistical and normalization errors. The two-body

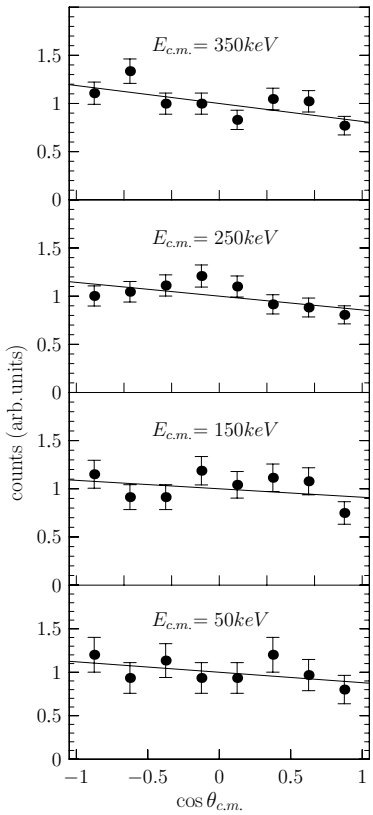

FIG. 9. Example of the angular distributions extracted at different $E_{\text{c.m.}}$ via the THM (dots). The solid lines through the data points are χ^2-fit using linear function [9].

angular distribution is in arbitrary unit and agrees with the behavior of the direct angular distribution [9].

A second validity test consists in the comparison between the behavior of the indirect excitation function and the direct one. Using Eq. (7), the quantity $(d\sigma/d\Omega)$ was extracted. The resulted two-body cross sections $\sigma(E)$ are shown in Fig. 10 (squares), where the direct data are also shown (open circles)

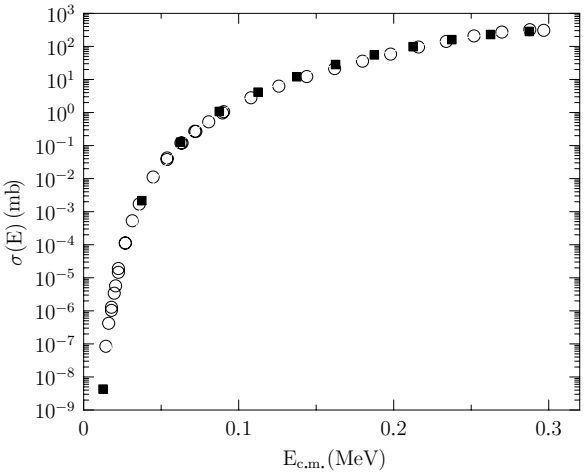

FIG. 10. Comparison between the THM indirect excitation function (squares) for the ^{9}Be$(p,\alpha)^6$Li reaction and the direct behavior (open circles) [9].

TABLE I. Astrophysical S factor for the ^{9}Be$(p,\alpha)^{6}$Li via the Trojan horse method.

$E_{\text{c.m.}}$ (MeV)	$S(E)$ (MeV b)	$\Delta S(E)$ (MeV b)
0.0125	20.7	4
0.0375	21.3	4
0.0625	26.3	5
0.0875	30.7	5
0.1125	33.8	5
0.1375	41.6	6
0.1625	51.0	7
0.1875	60.6	8
0.2125	71.9	9
0.2375	84.6	10
0.2625	91.7	11
0.2875	89.7	11

[9]. The normalization to direct behavior was performed in the energy range 75∼300 keV. The good agreement between the two data sets is a necessary condition for the further extraction of the astrophysical $S(E)$ factor by means of the THM.

V. RESULTS AND DISCUSSION

The extracted bare-nucleus $S(E)$ factor is shown in Fig. 11 as full squares and summarized in Table I. The direct data from Refs. [9,10] are also shown in Fig. 11. The behavior of the indirect $S(E)$ factor shows the presence of the expected low-energy resonance at $E_{\text{c.m.}} \sim 0.27$ MeV, corresponding to the 6.87 MeV, $J^{\pi} = 1^{-}$ level of ^{10}B. Both data sets show a similar energy dependence above ≈100 keV, while at lower energies the direct data exhibit a strong increase. This can be attributed to the electron screening effect, which is absent in the indirect measurement.

The $S(E)$ factor derived through the THM was fitted by a fifth-order polynomial of the form

$$S(E) = S(0) + S_1 E + S_2 E^2 + S_3 E^3 + S_4 E^4 + S_5 E^5. \quad (25)$$

The best fit is shown in Fig. 11 (solid line), and its coefficients are listed in Table II. We can see the extracted $S(E)$ factor $S(0) = 21.0 \pm 0.8$ MeV b.

The THM allows us to measure the bare astrophysical factor $S_b(E)$ [11], which can be compared with the screened (direct) value $S_d(E)$ to extract the associated screening potential energy U_e by the equation [9,11]

$$S_d(E) = S_b(E) \exp\left(\frac{\pi \eta U_e}{E}\right). \quad (26)$$

Using Eq. (26), we deduced the screening potential energy of $U_e = 676 \pm 86$ eV, which is much higher than the value one can expect from atomic physics models: $U_e \simeq 240$ eV (adiabatic limit [12]). And the result is lower than $Ue \simeq$ 830 eV, extracted from direct measurements with the inclusion of the $E_R = -26$ keV (i.e., $E_{\text{c.m.}} = -23$ keV) subthreshold resonance $\Gamma = 28$ keV in the data analyses in Ref. [9]. The subthreshold resonance corresponds to the 6.56 MeV level of ^{10}B.

TABLE II. Coefficients of the fifth-order polynomial fit for the $S(E)$ factor.

Coefficients	Value	Error
$S(0)$ (MeV b)	21.0	±0.8
S_1 (b)	−92.4	±13.4
S_2 (MeV^{-1} b)	4669	±78.5
S_3 (MeV^{-2} b)	-4.413×10^{4}	±331
S_4 (MeV^{-3} b)	2.193×10^{5}	±1251
S_5 (MeV^{-4} b)	-3.768×10^{5}	±3483
χ^2/ndf	5.3/6	

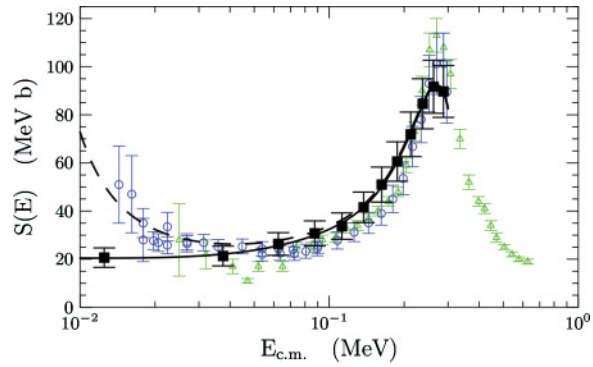

FIG. 11. (Color online) Bare-nucleus astrophysical $S(E)$ factor extracted via the THM (full squares) compared with the direct one (open circles [9] and open triangles [10]); a fit to the indirect data with a fifth-order polynomial [Eq.(25)] is also shown as a solid line. The fit to determine U_e is shown as a dashed line.

ACKNOWLEDGMENTS

The authors thank Lin Chengjian's group for helping us set up the target chamber, Xu Guoji in providing us with strip targets, and Li Xia in data acquisition. They also thank the technical staff of the Beijing Tandem Accelerator National Laboratory for their invaluable assistance, and also acknowledge support by the National Natural Science Foundation of China (10575132).

[1] R. N. Boyd and T. Kajino, Astrophys. J. **336**, L55 (1989).
[2] C. Rolfs and W. S. Rodney, *Cauldrons in the Cosmos* (University of Chicago, Chicago, 1988).
[3] G. Baur, Phys. Lett. **B178**, 135 (1986).
[4] S. Typel and G. Baur, Ann. Phys. (NY) **305**, 228 (2003).
[5] S. Romano *et al.*, Eur. Phys. J. A **27**, 221 (2006).

[6] M. Zadro, D. Miljanic, C. Spitaleri, G. Calvi, M. Lattuada, and F. Riggi, Phys. Rev. C **40**, 181 (1989).
[7] C. Spitaleri *et al*., Phys. Rev. C **69**, 055806 (2004).
[8] M. Jain *et al*., Nucl. Phys. **A153**, 49 (1970).
[9] D. Zahnow *et al*., Z. Phys. A **359**, 211 (1997).
[10] A. J. Sierk and T. A. Tombrello, Nucl. Phys. A **210**, 341 (1973).
[11] C. Spitaleri *et al*., Phys. Rev. C **63**, 055801 (2001).
[12] C. Angulo *et al*., Z. Phys. A **345**, 231 (1993).